---

# Supporting Information

## Ultrafine intermetallic platinum-cobalt with contracted Pt−Pt pair for efficient acidic oxygen reduction reaction

Chudi Ni,[1] Xiaoxia Chen[1], Yiwen Chen[1], Shiyu Li[1], Tao Zhou[1], Jing Yang[1], Meihuan Liu,[2,*] and Hui Su[1,*]

[1]*Key Laboratory of Light Energy Conversion Materials of Hunan Province College, College of Chemistry and Chemical Engineering, Hunan Normal University, Changsha 410081, Hunan, China*
[2]*State Key Laboratory for Powder Metallurgy, Central South University, Changsha 410083, Hunan, China*

* Corresponding author

E-mail: meihliu@csu.edu.cn; suhui@hunnu.edu.cn

E-

## 1. Materials

$CoCl_2 \cdot 6H_2O$, 2-MeIm, $CH_3OH$ and $C_3H_8O$ were purchased from Aladdin. $Zn(NO_3)_2 \cdot 6H_2O$, $H_2SO_4$ and $HClO_4$ were purchased from Sinopharm Chemical Reagent Co., Ltd. $H_2PtCl_6 \cdot 6H_2O$ was purchased Beijing HwrkChemical Technology Co., Ltd. Nafion (5 wt %) was purchased from Dupont. The commercial Pt/C (20 wt%) was purchased from Shanghai Macklin Biochemical Technology Co., Ltd. The distilled deionized water ($18.2\ M\Omega \cdot cm^{-1}$) applied in all experiments was obtained through an ultra-pure water system. All chemicals were employed directly without further purification.

## 2. Characterizations

### 2.1 Morphology and structure

To determine the crystal phase of catalysts, the powder X-ray diffraction (XRD) was performed using a Ultima IV X-ray diffractometer equipped with Cu Kα radiation source ($\lambda$=1.54178 Å). The morphology samples were analyzed via scanning electron microscopy (SEM) TESCAN. More accurate morphologies and nanoparticle size distribution were obtained by transmission electron microscopy (TEM) TESCAN. Thermo Scientific K-Alpha was utilized for conducting X-ray photoelectron spectroscopy (XPS), and the binding energy data were meticulously calibrated utilizing C 1s (284.4 eV). The contents of Pt and Co were detected by an inductively coupled plasma optical emission spectrometer (ICP-OES, Agilent 7700/7800).

### 2.2 X-ray Absorption Fine Structure Characterizations

The BL14W1 beam line at Shanghai Synchrotron Radiation Facility (SSRF) was explicitly utilized to conduct experiments on X-ray absorption spectroscopy (XAS), focusing on the Pt $L_3$-edge and Co K-edge. The Si (311) double-crystal monochromator was employed, and the results were obtained using a Lytle detector filled with Argon gas in fluorescence mode. Pt foil and Co foil were adopted as comparison samples. The collected data were manipulated via the Demeter software package, including Athena, Artemis, and Hephaestus. *In situ* XAFS measurements, the $Pt_3Co$ catalyst-coated carbon cloths was selected as working electrode in an acid solution by a homemade cell through a three-electrode system. Specifically, the 5 mg sample was evenly dispersed in 1 mL solution (water/ethanol = 3:1, v/v) containing 30 μLNafion. Then, the catalyst ink was deposited as the working electrode on the carbon paper (~1 cm × 1 cm), with the Capton film fixed on the back of the carbonpaper toensure thatmoreopening sites canparticipate in ORR. The representative potentials (1.00–0.70 V) were selected toobtain the evolution of atomic and electronic structure of the Pt sites during the ORR. When collecting XAFS measurement data, we used a Pt foil standard sample to calibrate the position of the absorption edge ($E_0$), and collected all XAFS data over a beam time period. We used a Lytle detector (fluorescence mode) to record XAFS spectra during electrochemical reactions.

### 2.3 Synchrotron Radiation Infrared Spectroscopy

We conducted *in situ* SRIR measurements at the beamline BL01B of the National Synchrotron Radiation Laboratory (NSRL, China). In order to gain better infrared signals, electrochemical tests were performed in a homemade top-plate cell. Specifically, considering the vibration absorption of water molecules, we used a ZnSe crystal window and pressed the catalyst electrode close to the window to reduce the loss of infrared light. The SRIR tests were employed in reflection mode with a spectral resolution of 2 $cm^{-1}$. Systemic ORR measurements were made after the background spectrum of the catalyst electrode was measured at an open-circuit voltage, and the ORR potential ranged from 1.00 to 0.50 V.

### 2.4 Electrochemical measurements

The electrocatalytic performance of each catalyst was measured via the rotating ring-disk electrode (RRDE) measurements (CHI760e, Shanghai Chenhua Instrument, China) with three-electrode system in 0.1 M $HClO_4$ at room temperature, in which the catalyst-coated glassy-carbon electrode as the working electrode (WE), the home-made RHE as the RE, and the carbon rod as the counter electrode. Firstly, 5 mg catalysts were dispersed in 1000 μL mixed solution (V (DI-water) : V (ethanol) : V (5% Nafion solution) = 3:1:0.3) and ultrasonicated for 0.5 h. Afterward, a certain amount of ink was added dropwise to the glassy-carbon electrode (GCE, 2 mm inner diameter, 0.1256 $cm^2$) and dried naturally at 25 °C. The mass loading of as-prepared catalysts was 0.39 mg $cm^{-2}$, and the loading of Pt for the Pt/C was 79 $\mu g_{Pt}$ $cm^{-2}$. Next, the catalysts were activated via cyclic voltammetry (CV). Subsequently, the electrocatalytic ORR performance was tested by steady-state measurement through the staircase voltammetry (SCV) tests. The stability of catalysts was also assessed by cycling the potential from 0.6 to 1.0 V (vs. RHE) at a scan rate of 100 mV $s^{-1}$ in $O_2$-saturated 0.1 M $HClO_4$.

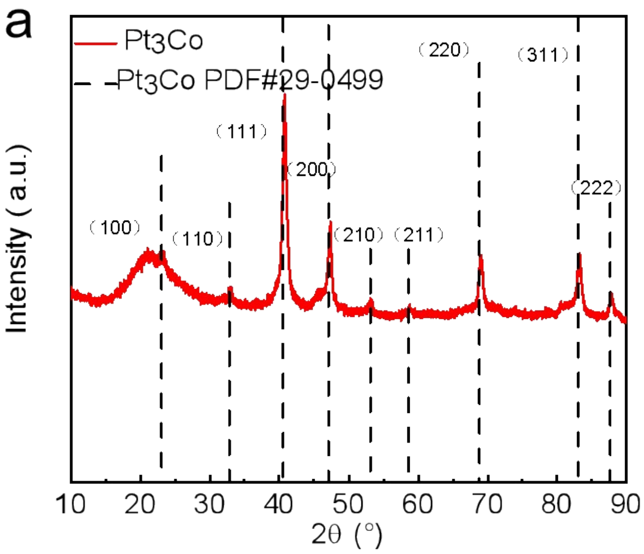

**Fig. S1** XRD pattern of $Pt_3Co$/NC

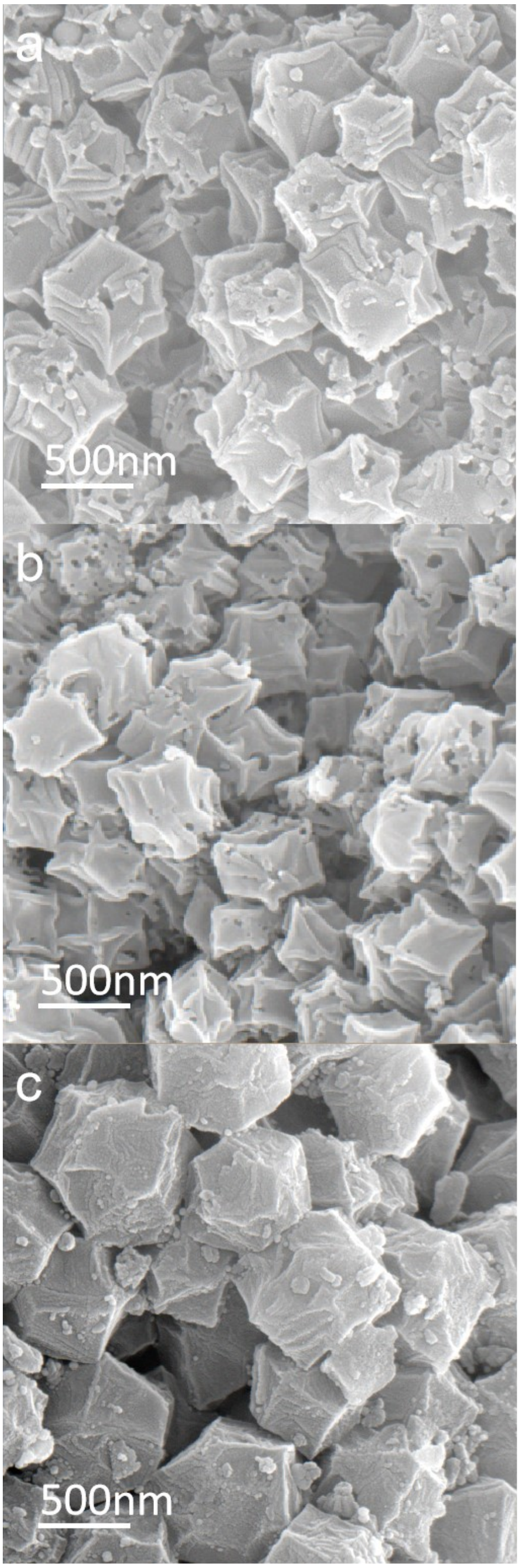

**Fig. S2** SEM images of (a) NC for acid leaching, (b) Co/NC and (c) Pt/NC catalysts

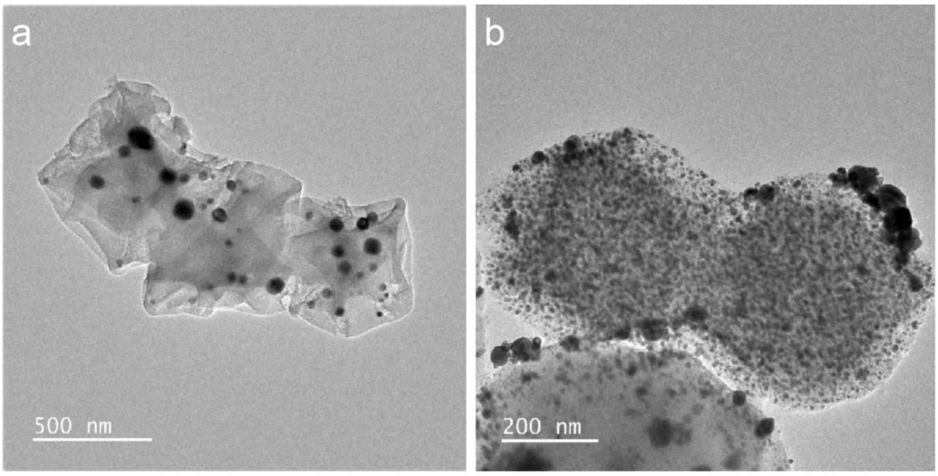

**Fig. S3** TEM images of (a) Co/NC and (b) Pt/NC catalysts

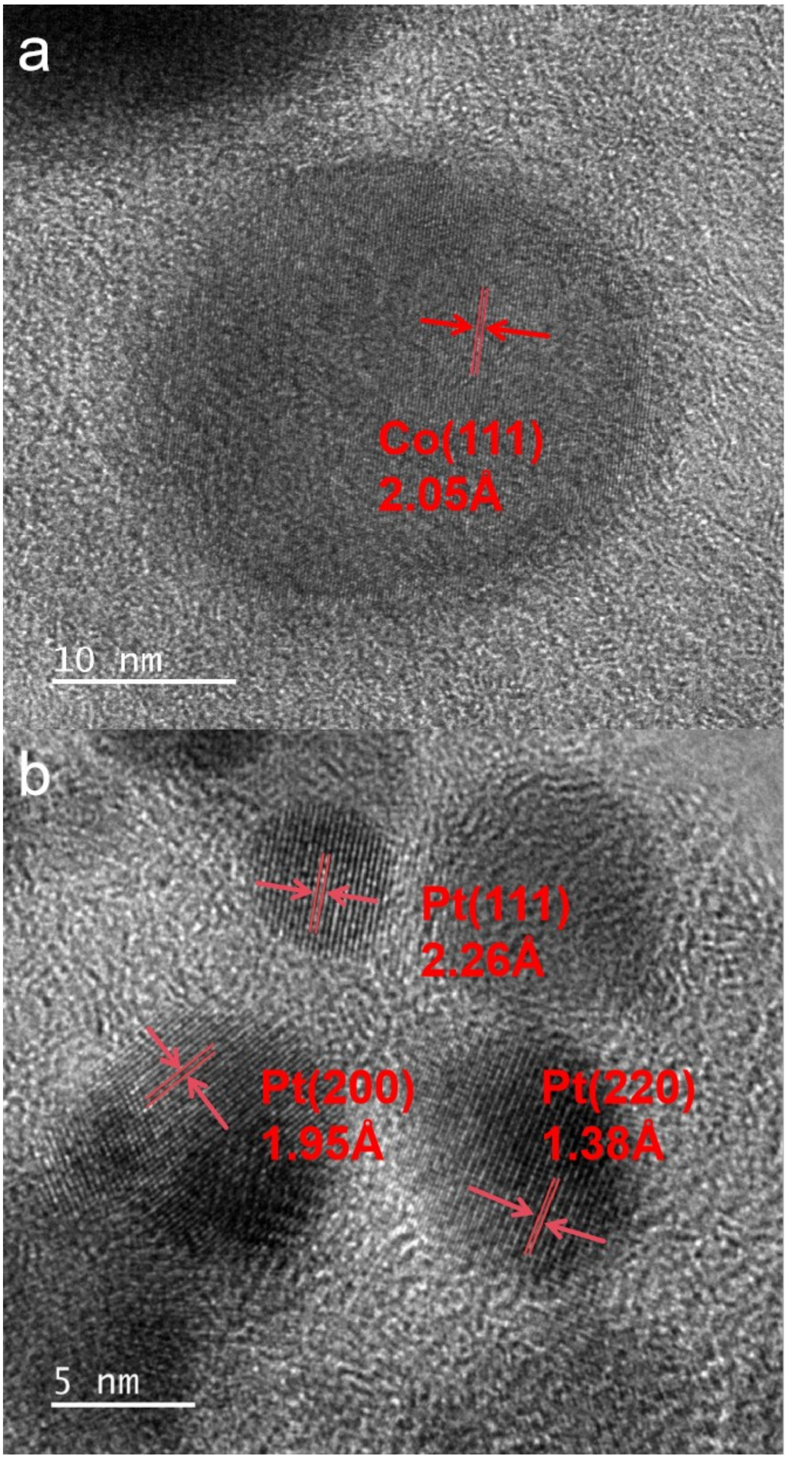

**Fig. S4** HRTEM images of (a) Co/NC and (b) Pt/NC catalysts

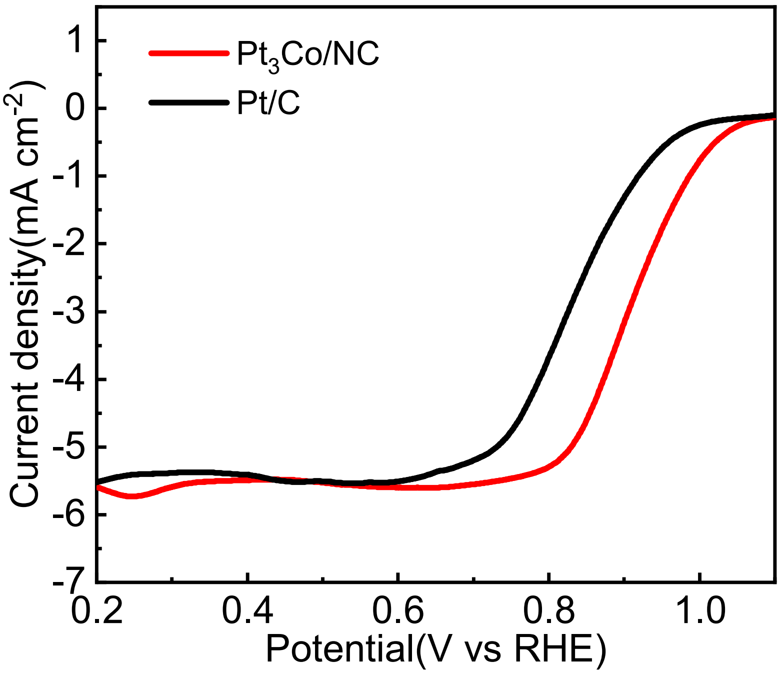

**Fig. S5** Steady-state polarization curves for the ORR in $O_2$-saturated 0.1 M KOH at room temperature with a rotation speed of 1600 rpm: Pt/C and $Pt_3Co$/NC.

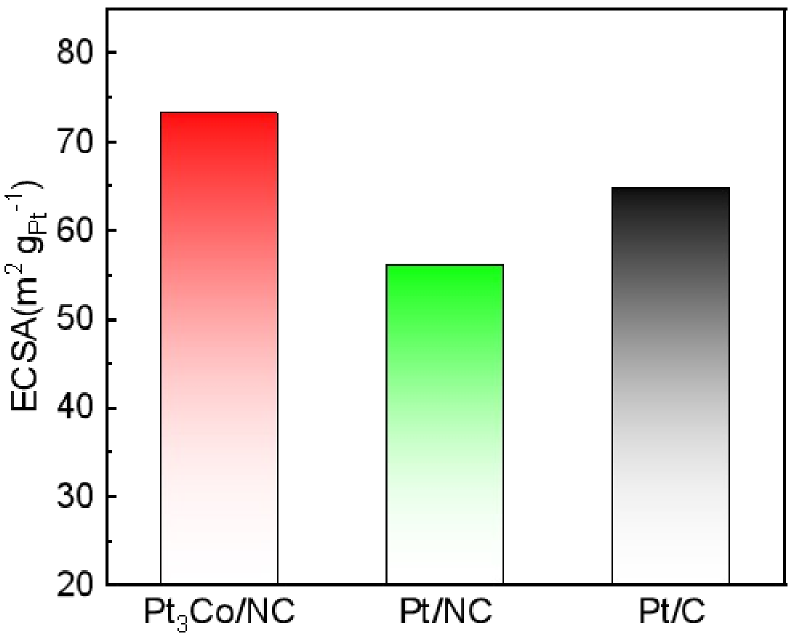

**Fig. S6** ECSA values calculated from CV.

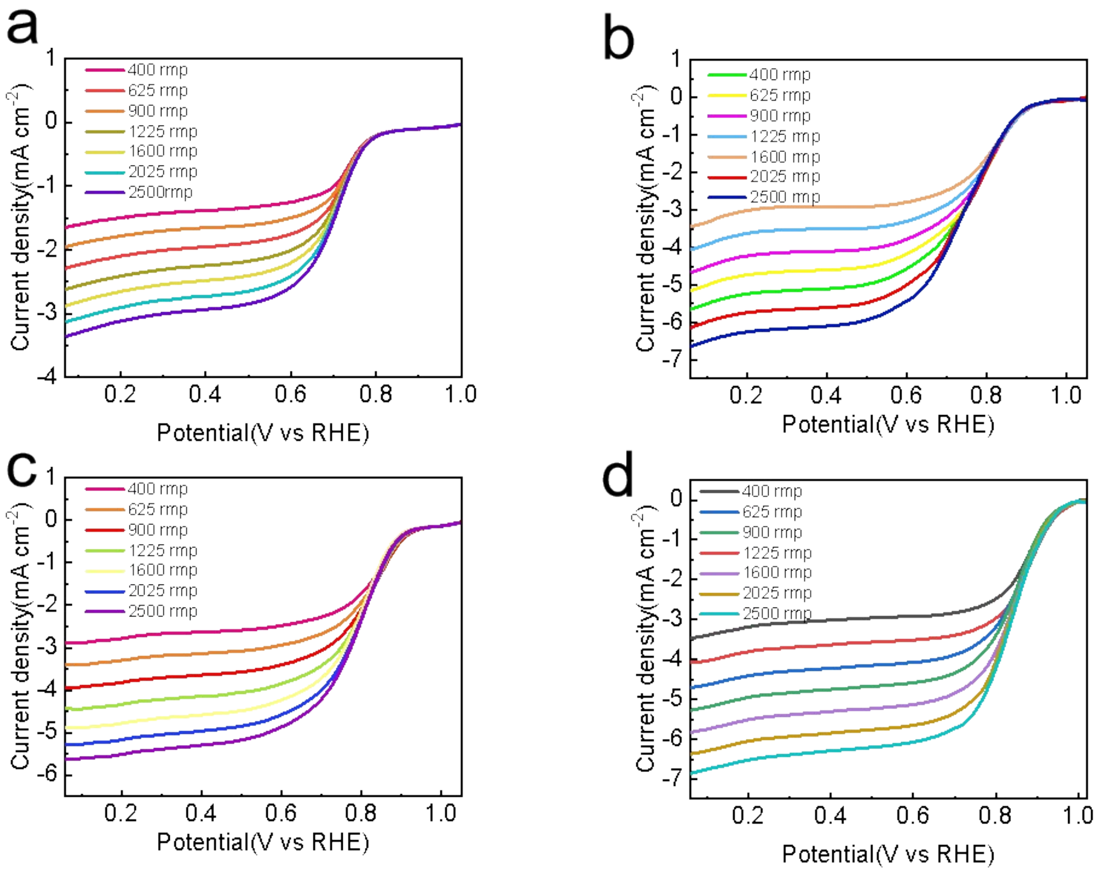

**Fig. S7** LSV curves at various rotation rates of (a) Co/NC, (b) Pt/C, (c) Pt/NC and (d) $Pt_3Co$/NC.

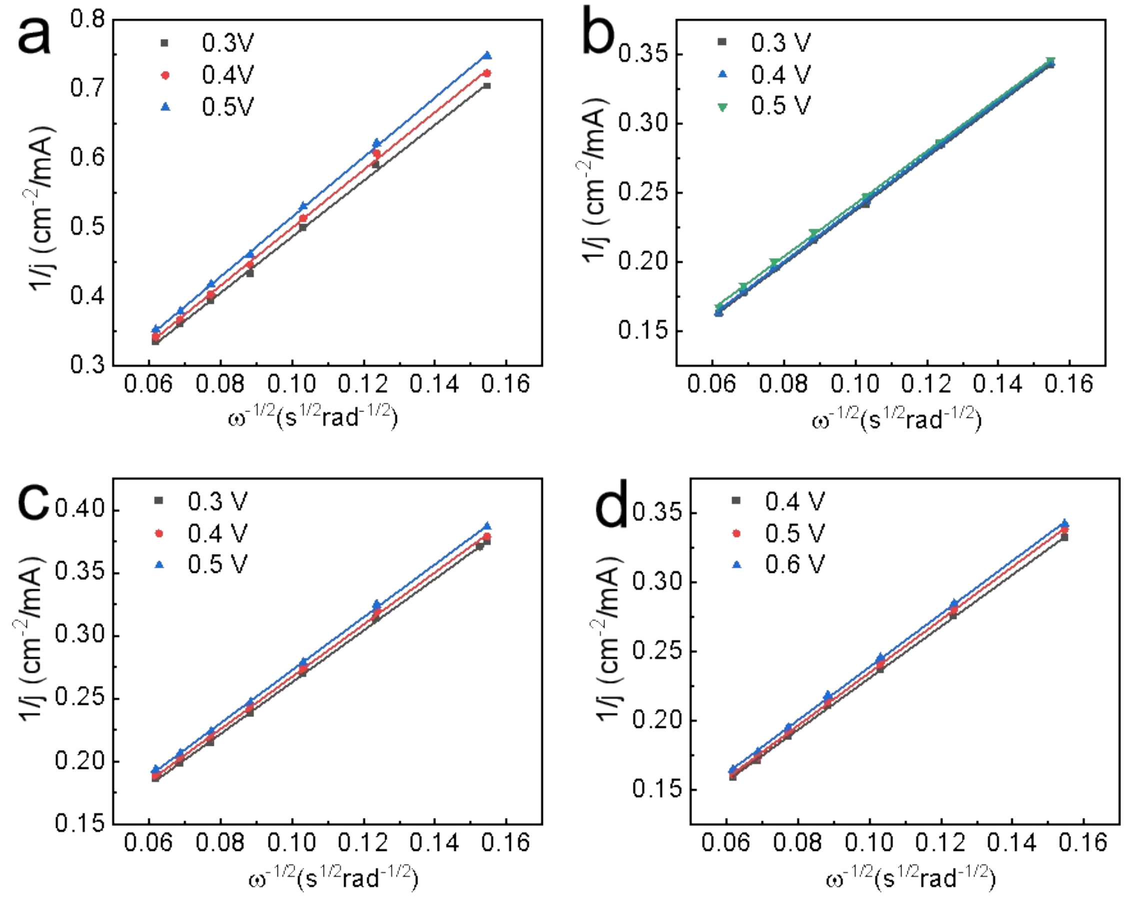

**Fig. S8** Corresponding Koutecky-Levich plots of (a) Co/NC, (b) Pt/C, (c) Pt/NC and (d) Pt$_3$Co/NC.

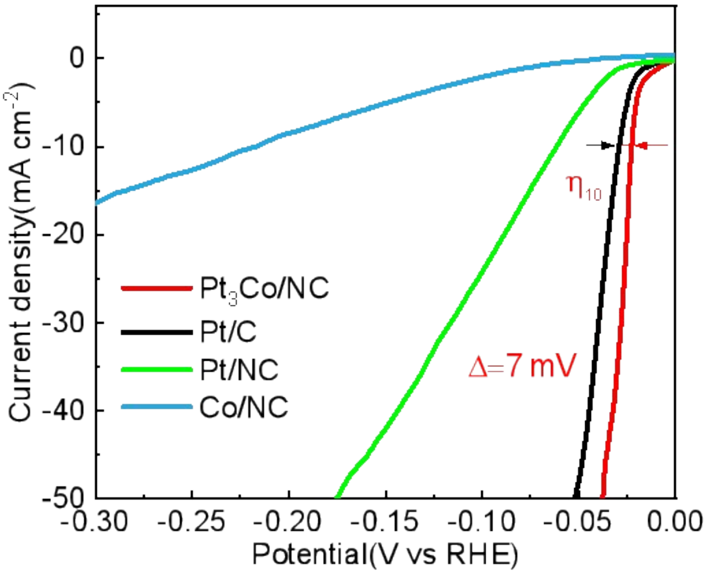

**Fig. S9** HER polarization curves of Co/NC, Pt/NC, $Pt_3Co$/NC and Pt/C in 0.5 M $H_2SO_4$ electrolyte at a scan rate of 5 mV $s^{-1}$.

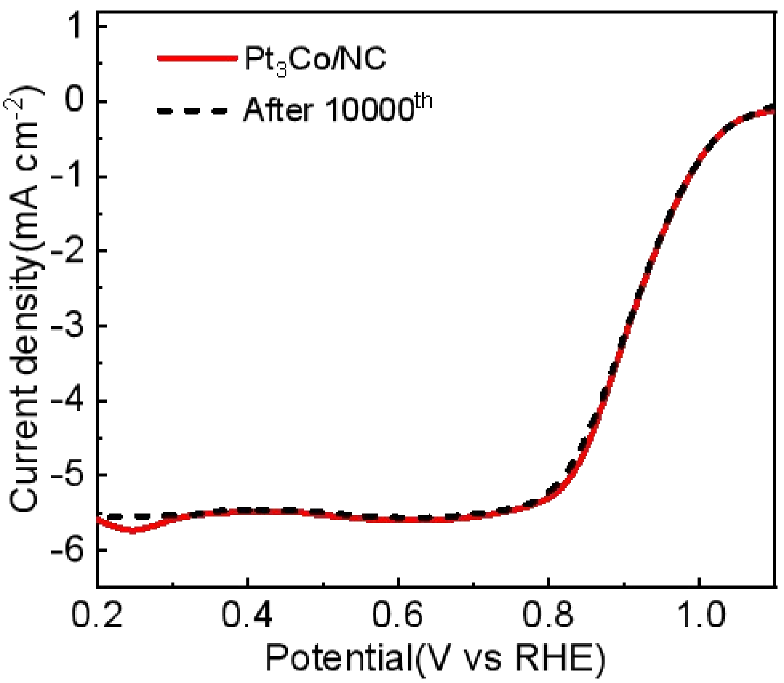

**Fig. S10** ORR polarization curves of Pt$_3$Co/NC before and after 10000 cycles (O2-saturated, 0.1 M KOH, 1600 r.m.p.).

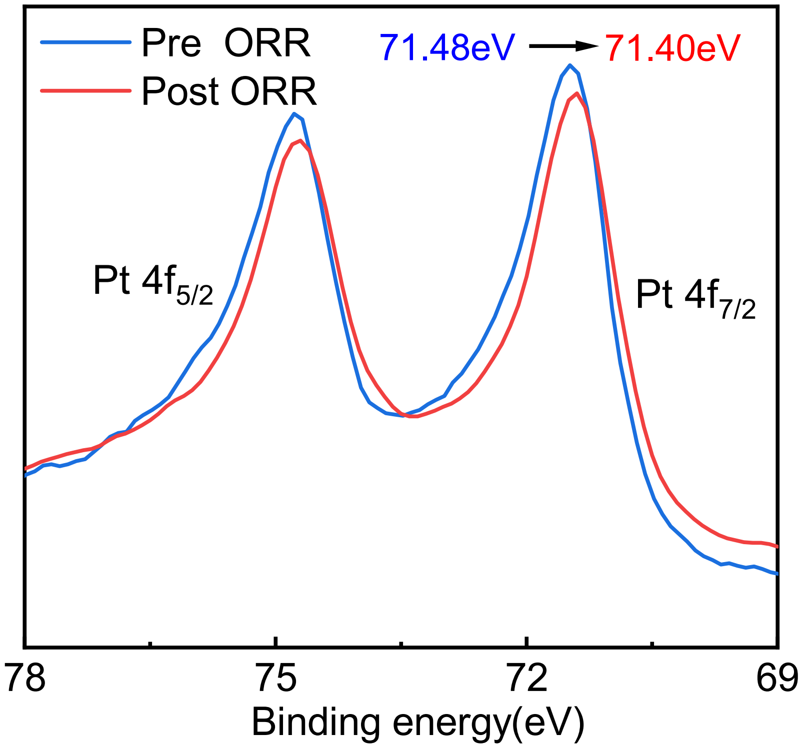

**Fig. S11** XPS spectra of the Pt 4f edge before and after the ORR.

**Table S1.** Comparison of the ORR performance for recently reported Pt electrocatalysts.

| **Catalysty** | **Pt wt%** | **Size (nm)** | **ECSA (m$^2$ g$^{-1}$)** | **E$_{1/2}$ (V)** | **Loss of E$_{1/2}$ (mV) after ADTs** | **Ref.** |
|---|---|---|---|---|---|---|
| Pt$_3$Co/NC | 14.5 | 4.18±1.00 | 73.16 | 0.89 | 14 (10 k) | This work |
| PtCo-9/NC | 17 | N/A | 27.02 | 0.89 | 2 (5 k) | [1] |
| PtCo/NG-3500-600/900 | 6.2 | ~3 | N/A | 0.86 | 13 (5 k) | [2] |
| Pt$_3$Co/Co@-800 | 8 | 32±7 | N/A | 0.82 | 2 | [3] |
| PtCo/NCS-S | 24.4 | N/A | 34.6 | 0.90 | 11 (20 k) | [4] |
| L1$_2$-Pt$_3$Co/Co-N-C | 1.69 | 2.38±0.04 | 77.8 | 0.89 | 42 (10 k) | [5] |
| O-Pt$_3$Co-30%CeO$_2$/C | 26.68 | 4.29±0.03 | 76.09 | 0.89 | 2 (20 k) | [6] |
| Pt$_3$Co$_{0.8}$Sn$_{0.2}$ | 18.9 | N/A | N/A | 0.86 | 10 (24 h) | [7] |
| I-PtCo@CN | N/A | ~5 | 71.4 | 0.89 | 35.3 (30 k) | [8] |
| PtNi/NW$_{493K}$/C | 88 | N/A | 111 | 0.88 | 11 | [9] |
| PtNi/Ni-NC | 7.2 | ~2.9 | 137.03 | 0.82 | 15 (5 k) | [10] |
| Pt$_3$Co/PNEGF | 30 | N/A | 52 | 0.77 | 24 (10 k) | [11] |
| PtFe@Pt/C-400 | 39.6 | N/A | 40.2 | 0.90 | 24 (30 k) | [12] |
| Pt$_3$Fe/SWCNT | 39 | 4.55±1.19 | 80.3 | 0.88 | 3 (10 k) | [13] |
| PtFe/DCNT | 1.7 | N/A | N/A | 0.84 | N/A | [14] |
| PtFe@Fe$_{SAs}$-N-C | 6.97 | 2.46±0.17 | N/A | 0.87 | 9 (30 k) | [15] |
| Pt$_3$Co@Mn$_{SA}$-NC | N/A | ~3 | 77.5 | 0.95 | 10 (30 k) | [16] |
| PtCo@NCS/BP-NH$_2$ | 18.36 | 3.9±0.79 | 57.3 | 0.91 | N/A | [17] |

1. M. Zhang, T. Zhou, D. Bukhvalov, F. Han, C. Wang and X. Yang, *Appl. Catal., B*, 2023, **337**.
2. L. Sun, Y. Qin and Y. Yin, *J. Power Sources*, 2023, **562**.
3. J. Liu, J. Zhang, M. Xu, C. Tian, Y. Dong and C.-A. Wang, *Inorg. Chem.*, 2022, **61**, 19309-19318.
4. K. Wan, H. Chen, J. Wang, B. Li, M. Chai, P. Ming and C. Zhang, *J. Catal.*, 2023, **427**.
5. M.-Y. Chen, S. Yin, G. Li, J. Chen, W.-Y. Zhao, Y.-K. Lian, H.-R. Wu, W. Yan, J.-N. Zhang and B.-A. Lu, *ACS Nano*, 2024, DOI: 10.1021/acsnano.4c06615.
6. H. Wang, J. Liu, K. Du, X. Wang, X. Li, Y. Liu, C. Min, F. Liu and X. Yang, *J. Power Sources*, 2024, **616**.
7. R. Yang, C. Dai, L. Zhang, R. Wang, K. Yin, B. Liu and Z. Chen, *J. Energy Chem*, 2024, **98**, 169-179.
8. Y. Gao, T. Uchiyama, K. Yamamoto, T. Watanabe, S. Tominaka, N. Thakur, R. Sato, T. Teranishi, H. Imai, Y. Sakurai and Y. Uchimoto, *ACS Catal.*, 2023, **13**, 10988-11000.
9. Y. Zhuang, Y. Iguchi, T. Li, M. Kato, Y. A. Hutapea, A. Hayashi, T. Watanabe and I. Yagi, *ACS Catal.*, 2024, DOI: 10.1021/acscatal.3c04709, 1750-1758.
10. G. Wang, J. Zhao, X. Chen, L. Niu, W. Zhang and X. Wang, *Int. J. Hydrogen Energy*, 2024, **64**, 309-317.
11. N. Manna, M. Singh and S. Kurungot, *ACS Appl. Mater. Interfaces*, 2023, **15**, 28023-28035.
12. E. Lee, D.-J. Lee, Y. Kim, C. Kim, Y. Kwon, H. Lee, I. Lim, B.-S. An, T.-H. Yang and G.-G. Park, *J. Alloys Compd.*, 2023, **968**.
13. J. He, C. Chen, H. Yu, Y. Zhao, M. Xu, T. Xiong, Q. Lu, Z. Yu, K. Tai, J. Tan and C. Liu, *J. Mater. Sci. Technol.*, 2024, **212**, 139-147.
14. S. Zeng, B. Lv, J. Qiao, W. Yang, C. Zhu, Y. Zhang, D. Hu, M. Chen, J. Di and Q. Li, *ACS Appl. Nano Mater.*, 2019, **2**, 7870-7879.
15. D. Xue, Y. Yuan, Y. Yu, S. Xu, Y. Wei, J. Zhang, H. Guo, M. Shao and J.-N. Zhang, *Nat. Commun.*, 2024, **15**.
16. Y. Zeng, J. Liang, C. Li, Z. Qiao, B. Li, S. Hwang, N. N. Kariuki, C.-W. Chang, M. Wang, M. Lyons, S. Lee, Z. Feng, G. Wang, J. Xie, D. A. Cullen, D. J. Myers and G. Wu, *J. Am. Chem. Soc.*, 2023, **145**, 17643-17655.
17. K. Wan, C. Luo, J. Wang, H. Chen, J. Zhang, B. Li, M. Chai, P. Ming and C. Zhang, *ACS Catal.*, 2024, **14**, 10181-10193.